Spin−Orbit Relativistic Time-Dependent Density Functional Calculations of the Metal and Ligand Pre-Edge XAS Intensities of Organotitanium Complexes: $TiCl_4$, $Ti(\eta^5\text{-}C_5H_5)Cl_3$, and $Ti(\eta^5\text{-}C_5H_5)_2Cl_2$

Maurizio Casarin,*,† Paola Finetti,† Andrea Vittadini,§,|| Fan Wang,+ and Tom Ziegler*,‡

Dipartimento di Scienze Chimiche, Università degli Studi di Padova, Padova, Italy, Istituto di Scienze e Tecnologie Molecolari del CNR, Padova, Italy, Consorzio Interuniversitario di Scienza e Tecnologia dei Materiali, Firenze, Italy, Department of Chemistry, University of Hong Kong, Hong Kong, China, and Department of Chemistry, University of Calgary, Calgary, Alberta, Canada T3A1N4

Received: February 26, 2007; In Final Form: April 11, 2007

Time-dependent density functional theory (TDDFT) coupled to the relativistic two-component zeroth-order regular approximation, both available in the last version of the ADF package, have been successfully used to simulate X-ray absorption spectra of $TiCl_4$, $Ti(\eta^5\text{-}C_5H_5)Cl_3$, and $Ti(\eta^5\text{-}C_5H_5)_2Cl_2$ in terms of their oscillator strength distributions. Besides allowing a first principle assignment of Ti 1s, Cl 1s, and Ti 2p ($L_{2,3}$ edges) core excitation spectra, theoretical outcomes provide a rationale for deviations from the expected L_3/L_2 branching ratio.

1. Introduction

The bonding interaction between metal centers (M) and unsaturated ligands (L) was first described by Dewar[1] and by Chatt and Duncanson[2] on the basis of a two-way electron flow, i.e., a L → M charge transfer from ligand σ or π molecular orbitals (MO) into suitable virtual M-based levels assisted by a M → L back-donation from atom-like dπ atomic orbitals (AOs) into L π* virtual MOs. Since then, much work has been done in order to understand how the relative degree of donation and back-donation is affected by (i) the ancillary ligands bonded to M, (ii) the nature of L, (iii) the number of d electrons localized on M, and (iv) the relativistic effects.[3]

In the field of organometallic compounds, metallocene complexes of group IV metals have been the object in the near past of a growing attention.[4−5] Such an interest has to be ultimately traced back to two factors: (i) the catalytic activity of both mono- and bis-cyclopentadienyl titanium(IV) complexes;[5−7] (ii) the possible use of titanocene dichloride and its water soluble derivatives as possible alternatives to the widely used heavy metal based anticancer drugs.[9−10]

X-ray absorption spectroscopy (XAS) is unanimously recognized as a new experimental tool able to provide a site selective probe of molecular unoccupied electronic structure. XAS implies the excitation of core electrons to unoccupied valence orbitals as well as to the continuum, and its great advantage is related to the localized character of core excitations, thus making K- and L-edge[11] spectra very sensitive to both the electronic structure and the local surroundings of the absorbing atom. M K-edge studies focus on the electric dipole forbidden but quadrupole allowed[12−14] $1s^M \rightarrow nd^M$ transitions, which may be enhanced in non-centro-symmetric complexes through the involvement of metal *n*p AOs into frontier virtual MOs. In this regard it is worth of note that M K-pre-edge is sensitive to mixing on the 4p−3d order of 1%, thus supplying a quite accurate measurement of such a mixing. At variance to that, the potentially richer M L-edge structures are dominated by electric dipole allowed $2p^M \rightarrow nd^M$ transitions. They then probe the contribution of M *n*d AOs to the unoccupied electronic structure but without providing any information about specific M−L bonds.[15a] Also L K-edge absorptions imply electric dipole allowed transitions (the $1s^L \rightarrow np^L$), but since their intensity fits the virtual level L *n*p character, they are very well suited to measure the covalency degree of a specific M−L bond.[15]

The first Ti 1s excitation spectrum of $TiCl_4$ was recorded by Kuetgens and Hormes[16] at the beginning of the nineties. A few years later, Wen and Hitchcock[17] derived the oscillator strengths (*f*) for the C 1s excitation of gas-phase $Ti(\eta^5\text{-}C_5H_5)Cl_3$ (hereafter, $TiCpCl_3$) and $TiCp_2Cl_2$ as well as for the Cl 2p and Ti 2p excitations of $TiCl_4$, $TiCpCl_3$, and $TiCp_2Cl_2$ by means of electron energy loss spectroscopy under electric dipole scattering conditions. The authors assigned the C 1s excitation spectra by referring to empirical extended Hückel type (EHT) calculations, while the interpretation of the Ti 2p ones were based on both EHT results and atomic multiplet crystal field calculations for Ti^{4+}. Two years ago, Solomon et al.[18] reported Ti and Cl K-edge XAS data for $TiCl_4$, $TiCpCl_3$, and $TiCp_2Cl_2$, correlating them with ground state (GS) DFT calculations.[19] Their results confirmed that the Ti (Cl) K-pre-edge intensities can be used as a direct probe of the Ti 3d−4p mixing (Ti−Cl covalency).

The approach adopted by Solomon et al.[18] provides an exhaustive description of the M−L interactions and it results rather appropriate for the interpretation of experimental splittings and intensities. However, since a proper description of XA spectral features, in particular of the L-edge, needs both the inclusion of the configuration mixing in the calculations and the treatment of spin−orbit (SO) effects,[20−21] relativistic time-dependent density functional theory (RTDDFT) including SO coupling with full use of symmetry and correlation effects[22] represents a striking improvement with respect to single particle methods. Moreover, the treatment of core electron excitations

* Corresponding author.
† Università degli Studi di Padova.
‡ University of Calgary.
§ Istituto di Scienze Molecolari del CNR.
|| Consorzio Interuniversitario di Scienza e Tecnologia dei Materiali.
+ University of Hong Kong.

10.1021/jp071561g CCC: $37.00
Published on Web 05/25/2007

can take advantage of a scheme recently proposed by Stener et al.[20] which reduces the complete one-electron excited configurations space (1h−1p space) to the subspace where only the core electrons are excited. Both the SO-RTDDFT formalism and the Stener scheme are implemented in the latest version of the ADF program package. In this regard, it has to be mentioned that Fronzoni et al.[21] recently reported a case study devoted to the theoretical simulation of the $TiCl_4$ Ti 2p core excitations.

In this contribution we adopt the SO-RTDDFT approach to carry out a first principle study of the Ti 1s, Cl 1s, and Ti 2p core excitations of $TiCpCl_3$ and $TiCp_2Cl_2$ with the aim of gaining information about their molecular unoccupied electronic structure and further testing the potentiality of the SO-RTDDFT formalism when applied to rather complex molecular systems.

2. Computational Details

K- and L-edge XA spectra of the title molecules have been simulated by using the Amsterdam Density Functional (ADF) package.[23] We adopted the relativistic two-components zeroth-order regular approximation (ZORA)[24] and TDDFT[22] suitably tailored to treat core electron excitations.[20] This two-component TDDFT formalism has the correct nonrelativistic limit and affords the correct threefold degeneracy of triplet excitations.

Two-components ZORA SO-RTDDFT numerical experiments have been carried out by adopting all-electron QZ4P ZORA basis sets for all the atoms.[25] Two shells of diffuse functions, following the even tempered criterion, further augmented the QZ4P ZORA basis sets of Ti and Cl since it is well-known[21] that these kind of functions are needed to properly describe transitions toward Rydberg states. The adiabatic local density approximation[26] has been employed to approximate the XC kernel, while for the XC potential applied in the self-consistent field calculations, the LB94 approximate functional[27] with the GS electronic configuration has been adopted. In this regard, Fronzoni et al.[21] have pointed out that, among approximate XC functionals having the correct asymptotic behavior, a necessary condition for a proper description of high-energy virtual orbitals and Rydberg states, the LB94 functional is the one providing the best agreement between theory and experiment. Finally, scaled ZORA orbital energies[28] instead of the ZORA orbital energies in the TDDFT equations have been throughout employed to improve deep core excitation energies.

3. Results and Discussion

Solomon et al.[18] carried out GS DFT calculations for title molecules by using as initial input for their geometry optimization the corresponding crystal structure parameters. Moreover, they assumed a T_d symmetry for the $TiCl_4$ species, while no symmetry was imposed for $TiCpCl_3$ and $TiCp_2Cl_2$. Since the full use of symmetry in SO-RTDDFT calculations significantly reduces the computational effort while at the same time facilitating the assignments of spectral features,[22] we have run a series of preliminary nonrelativistic (NR) DFT calculations to evaluate molecular geometry, electronic structure and bonding energy differences between structures optimized by Solomon et al.[18] and those obtained by imposing a C_s and a C_{2v} symmetry to $TiCpCl_3$ and $TiCp_2Cl_2$, respectively (see Figure 1).[29] Obviously, basis sets (TZP) and XC functional (the approximation of Vosko et al.[30] with generalized gradient corrections self-consistently included through the Becke−Perdew[31] formula) were the same used in ref 18. Obtained results show that the above-mentioned differences are negligible. On this basis, SO-RTDDFT calculations have been run by assuming a C_s and a C_{2v} symmetry for $TiCpCl_3$ and $TiCp_2Cl_2$, respectively.

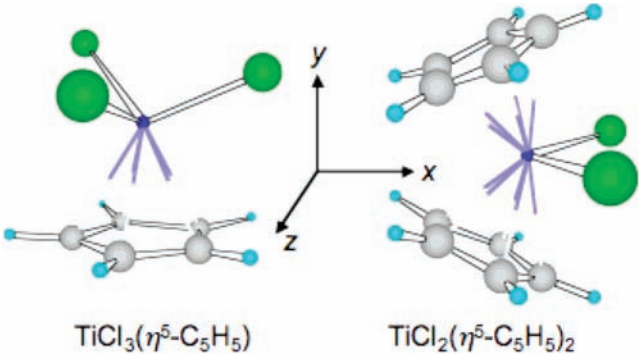

Figure 1. Schematic representation of $TiCpCl_3$ and $TiCp_2Cl_2$ with C_s and C_{2v} symmetry, respectively.

Ti K-edges. In the T_d, C_s, and C_{2v} symmetry point groups, the electric-dipole moment operator transforms as the t_2 (T_d), $a' + a''$ (C_s), and $a_1 + b_1 + b_2$ (C_{2v}) irreducible representations. Electric dipole allowed transitions from the totally symmetric Ti 1s core level need then to span the same representations.[32−33] Starting with the tetrahedral $TiCl_4$ molecule, we note that the unoccupied frontier orbitals (3e and $10t_2$ MOs) have a strong Ti 3d AOs contribution and a Ti−Cl antibonding character (the GS charge density analysis of title molecules is not herein reported because, as already mentioned, it perfectly matches those of ref 18). On this basis, both Kuetgens & Hormes[16] and Solomon et al.[18] assigned the Ti K-pre-edge feature centered at 4969.15 eV (**X** in Figure 2, capital and small bold character label experimental and theoretical features, respectively) to the $1a_1 \rightarrow 10t_2$ transition,[34−35] while the feature **Y** at 4976.75 eV was ascribed by means of NR TDDFT calculations[20] to three closely spaced Rydberg transitions whose intensities reflect the Ti 4p character of the 11, 13 and 14 t_2 MOs.

The SO coupling has no effect on the Ti 1s initial state (IS) and a single spinor, the $1e_{1/2}$ in the T_d* double group, is thus generated. Moreover, transitions allowed by the electric dipole selection rules are the $e_{1/2} \rightarrow u_{3/2}$ and $e_{1/2} \rightarrow e_{5/2}$ ones.[33] The simulated distribution of *f* is compared with the Ti 1s excitation spectrum of $TiCl_4$ in Figure 2, while theoretical excitation energies and corresponding intensities are collected in Table 1, where two component relativistic final state (TC-RFS) and scalar RFS (S-RFS) compositions are also included.

The inspection of Table 1 testifies that the first and the second excitations are quasi-degenerate (4951.1 eV) and have the same S-RFS ($10t_2$). Analogous considerations hold for the third and fourth excitations which lie at 4956.9 eV and have the $11t_2$ MO as S-RFS. In this regard, it has to be mentioned that a t_2 singlet state can only give rise to one t_2 excited-state in a double ground representation, so that the above-mentioned quasi-degeneracy could be due to a quasi-degeneracy between singlet and triplet S-ZORA core excitation energies for some t_2 states. Numerical experiments carried out within the S-ZORA TDDFT approach confirmed that the singlet−singlet and singlet−triplet excitation energies are indeed almost the same thus explaining the near degeneracy in the SO-RTDDFT results.

The energy region below the theoretical Ti 1s ionization limit[34] is characterized by the presence of four peaks at 4951.1 (**x**), 4956.9 (**y**), 4958.3 (**z**), and 4959.0 (**t**) eV (see Figure 3). Data reported in Table 1 allow us to associate **x** to the $1e_{1/2} \rightarrow (10e_{5/2} + 15u_{3/2})$ transition reminiscent of the NR $1a_1 \rightarrow 10t_2$ one, while the closely spaced **y**, **z**, and **t** peaks relate to Ti 1s $\rightarrow$ 4p Rydberg transitions (**y** and **t**) as well as to excitations significantly involving Cl 3d AOs besides the Ti 4p ones (z). Furthermore, taking the energy of **x** as a reference, the relative

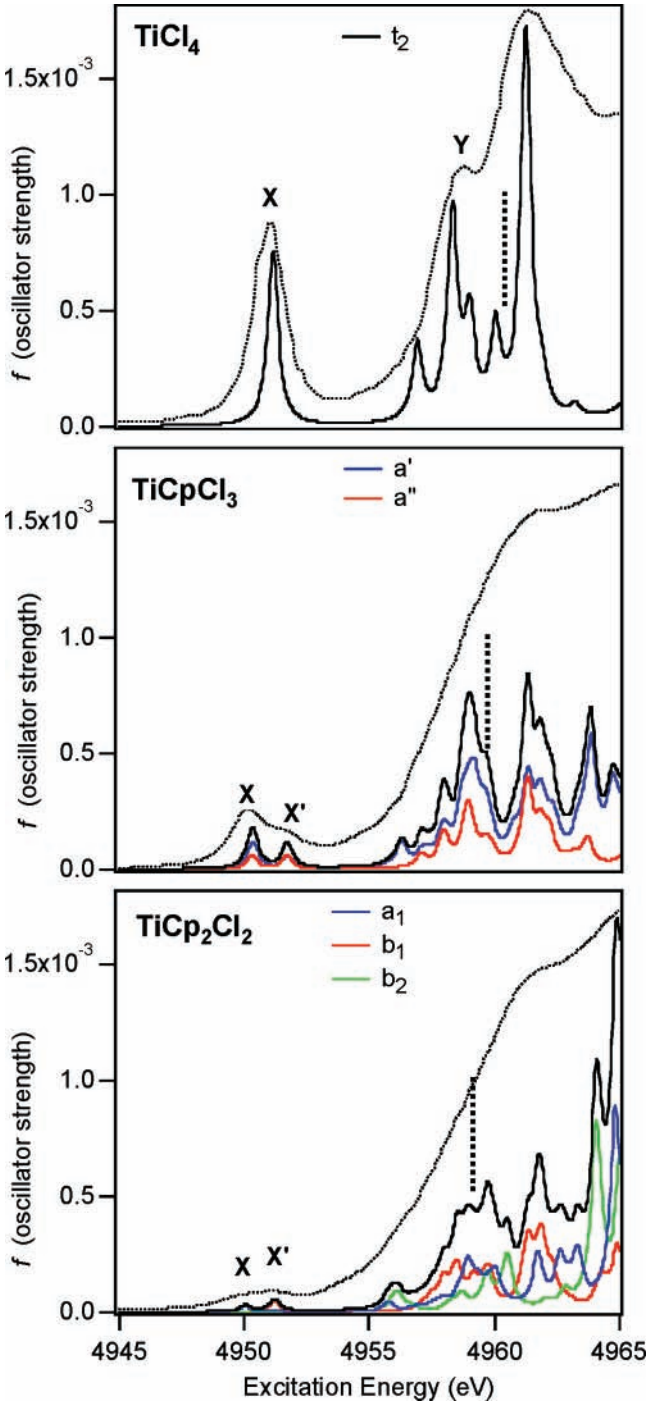

Figure 2. SO-RTDDFT LB94-GS Ti 1s excitation spectra of $TiCl_4$, $TiCpCl_3$, and $TiCp_2Cl_2$. Corresponding electric dipole allowed components are also displayed. Convoluted profiles have been obtained by using a Lorentzian broadening of 0.25 eV. Experimental curves (dashed lines) are taken from refs 16 ($TiCl_4$) and 18 ($TiCpCl_3$ and $TiCp_2Cl_2$), and they are all red-shifted by 18 eV to allow the matching between the lowest lying theoretical and experimental features. Vertical dotted lines indicate the calculated ionization limits (4960.5, 4959.8, and 4959.2 eV in $TiCl_4$, $TiCpCl_3$, and $TiCp_2Cl_2$, respectively).

position of **y** (**z** and **t**) matches rather well the experimental value of the rising edge onset (the sharp resonance **Y**).[16]

On passing from $TiCl_4$ to $TiCpCl_3$, the experimental Ti K-pre-edge feature (see Figure 2) is characterized by: (i) a significant decrease in the relative intensity (by a factor ~2); (ii) the splitting of $\mathbf{X}^{TiCl_4}$ in two components, **X′** and **X″**, lying at 4968.1 and 4969.5 eV, respectively, with an intensity ratio ($\rho_{\mathbf{X'/X''}}$) equal to 2.3;[18,36] iii) a red shift involving both **X′** ($\Delta E_{\mathbf{XX'}} = 1.04$ eV) and the onset of the rising edge.

Again, the inspection of Figure 2 and 3 confirms the good agreement between theory and experiment. More specifically, (i) the low excitation energy region of the simulated $TiCpCl_3$ Ti 1s spectrum is characterized by the presence of the peaks **x′** and **x″**, with **x′** red-shifted by 0.8 eV with respect to $\mathbf{x}^{TiCl_4}$, (ii) $\Delta E_{\mathbf{x''x'}} = 1.4$ eV, (iii) $(f_{\mathbf{x}})^{TiCl_4}/(f_{\mathbf{x'}} + f_{\mathbf{x''}})^{TiCpCl_3} = 2.48$, and (iv) $(f_{\mathbf{x'}}/f_{\mathbf{x''}})^{TiCpCl_3} = 1.53$. Furthermore, on passing from $TiCl_4$ to $TiCpCl_3$ the Ti 1s ionization limit is red-shifted by 0.7 eV.

Before tackling the detailed assignment of the $TiCpCl_3$ Ti 1s excitation spectrum, it can be useful to emphasize a few points about its electronic structure. There is no doubt that, on passing from $TiCl_4$ to $TiCpCl_3$, the overall molecular symmetry is reduced from T_d to C_s; on the other hand, the quasi-octahedral environment of the Ti atom in the $TiCpCl_3$ molecule[37] allows us to recognize t_{2g}-like (d_{z^2}, d_{xz}, and $d_{x^2-y^2}$ orbitals in the selected framework—see Figure 1) and e_g-like (d_{xy} and d_{yz} orbitals) components in the splitting of the Ti 3d AOs. According to that, the correlation diagram reported in Figure 4 testifies that, moving from $TiCl_4$ to $TiCpCl_3$, Ti 3d empty AOs are not only shifted toward higher energies as a consequence of the substitution of a chloride anion (a two electron donor) with the cyclopentadienyl one (a six electron donor), but the quasi-octahedral crystal field reverses their splitting and, at the same time, increases their energy difference. Such a picture agrees very well with experimental findings which provide a measurement of the energy difference ($\Delta E_{\mathbf{X''X'}}$) between t_{2g}-like (21a″ + 35a′ + 36a′ SR MOs) and e_g-like (22a″ + 37a′ SR MOs) virtual levels.

A thorough analysis of TC-RFS and S-RFS compositions of $TiCpCl_3$ excitation energies (see Table 2) clearly states that low-lying excitations can be divided in two sets, the former (latter) corresponding to transitions toward $55\varphi_{1/2}-57\varphi_{1/2}$ ($58\varphi_{1/2}-59\varphi_{1/2}$) spinors related to the Ti t_{2g}-like (Ti e_g-like) orbitals and giving rise to the component **x′** (**x″**), both deriving from a significant mixing of excited configurations. Such an evidence confirms the inadequacy of the single particle approach in reproducing spectral features.

Analogously to $\mathbf{y}^{TiCl_4}$, both the **y′** and **y″** peaks of the simulated $TiCpCl_3$ Ti 1s spectrum are related to Ti 1s → 4p Rydberg excitations and represent the onset of the rising edge. In this regard, it has to be noted that, in agreement with experimental observations, **y′** lies at lower excitation energies than $\mathbf{y}^{TiCl_4}$ ($\Delta E_{\mathbf{yy'}} = 0.60$ eV). Moreover, according to data reported in Table 2, we propose to assign **y′** to the single $1\varphi_{1/2} \rightarrow 68\varphi_{1/2}$ excitation, and **y″** to the $1\varphi_{1/2} \rightarrow 69\varphi_{1/2}$ and $1\varphi_{1/2} \rightarrow 70\varphi_{1/2}$ ones. Incidentally, spinors $68\varphi_{1/2}$ are related to the SR 43a′ MO, which is strongly localized on the Ti $4p_x$ AO, while the $69\varphi_{1/2}$ and $70\varphi_{1/2}$ ones are linked to the SR 44a′ and 26a″ MOs, significantly concentrated on $4p_z$ and $4p_y$ AOs.

The substitution of a second chloride with a second cyclopentadienyl anion has three effects on the Ti K-pre-edge feature which consists, as in $TiCpCl_3$, of two peaks (**X′** and **X″**) placed at 4967.28 and 4968.7 eV, respectively:[18,38] (i) a further decrease in relative intensity (by a factor of ~6 with respect to $TiCl_4$),[35] (ii) an inversion of the intensity of the two peaks ($\rho_{\mathbf{X'/X''}} = 0.74$), (iii) a uniform shift of spectral features toward lower excitation energies (0.8 eV).[38]

The agreement between theory and experiment[18] is once more remarkable (see Figure 2 and 3). In more detail, our calculations yield (i) $\Delta E_{\mathbf{x''x'}} = 1.2$ eV, (ii) $(f_{\mathbf{x}})^{TiCl_4}/(f_{\mathbf{x'}} + f_{\mathbf{x''}})^{TiCp_2Cl_2} = 8.3$, and (iii) $(f_{\mathbf{x'}}/f_{\mathbf{x''}})^{TiCp_2Cl_2} = 0.57$. Moreover, the ΔE between the **x′** (**x″**) components in $TiCpCl_3$ and $TiCp_2Cl_2$ is 0.3 (0.5) eV,

TABLE 1: Excitation Energies (eV) and Oscillator Strengths *f* for the Ti 1s Excitation Spectrum of $TiCl_4$ from Two Components ZORA TD-DFT[a]

initial state	edge	*E* (eV)	Δ*E* (eV)	$f \times 10^4$	TCRFS (%)[b]	SRFS (%)[b]
$1s_{1/2}$ ($1e_{1/2}$)	K	4951.1	0.0	0.1033	$10e_{5/2}$ (86) + $15u_{3/2}$ (14)	$10t_2$ (100)
		4951.1	0.0	1.858	$10e_{5/2}$ (14) + $15u_{3/2}$ (86)	$10t_2$ (100)
		4956.9	5.8	0.1187	$11e_{5/2}$ (94) + $16u_{3/2}$ (6)	$11t_2$ (100)
		4956.9	5.8	0.7533	$11e_{5/2}$ (6) + $16u_{3/2}$ (94)	$11t_2$ (100)
		4958.3	7.2	2.249	$13e_{5/2}$ (18) + $19u_{3/2}$ (82)	$13t_2$ (100)
		4959.0	7.9	1.006	$14e_{5/2}$ (60) + $20u_{3/2}$ (40)	$14t_2$ (100)
		4960.0	8.9	0.9321	$15e_{5/2}$ (18) + $23u_{3/2}$ (82)	$15t_2$ (100)

[a] Only the t_2 excitations lying at energies lower than the edge are reported. The DFT-KS 1s ionization energy is 4960.5 eV. TCRFS and SRFS stand for two-component relativistic final state and scalar relativistic final state, respectively. [b] Only transitions having $f \times 10^4 \geq 0.1$ and contributions to the TCRFS/SRFS ≥ 1% are reported.

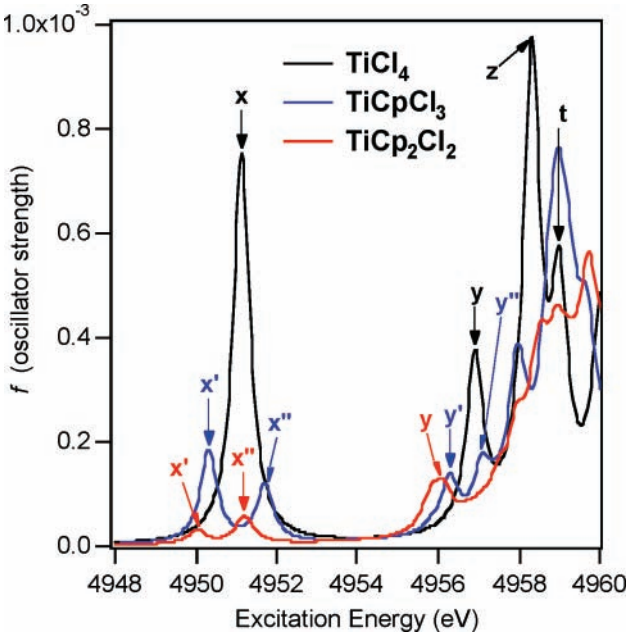

Figure 3. Superposition of the SO-RTDDFT LB94-GS Ti 1s excitation spectra of $TiCl_4$, $TiCpCl_3$, and $TiCp_2Cl_2$.

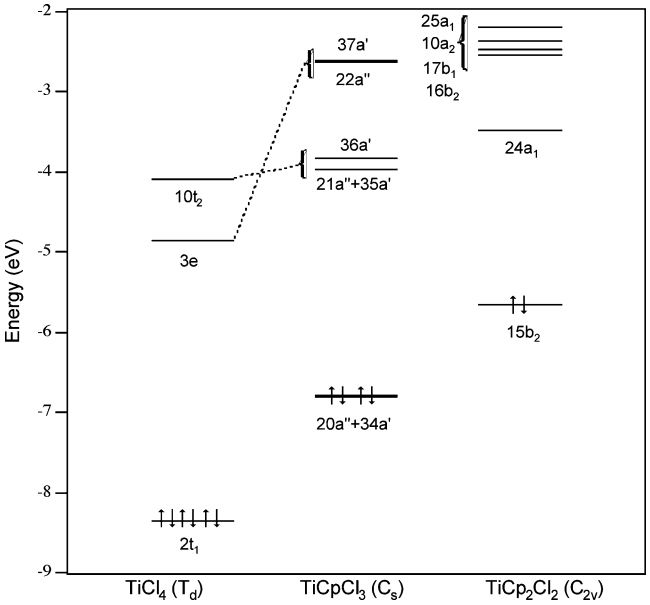

Figure 4. Correlation diagram of $TiCl_4$, $TiCpCl_3$, and $TiCp_2Cl_2$ frontier orbitals. Energy eigenvalues refer to optimized structures obtained by using the same basis sets and XC functional employed by Solomon et al. in ref 18.

and **y′** lies at lower excitation energies in $TiCp_2Cl_2$ than in $TiCpCl_3$. Finally, on passing from $TiCpCl_3$ to $TiCp_2Cl_2$ the Ti 1s ionization limit is red-shifted by 0.6 eV.

As already done for $TiCpCl_3$, it can be useful to examine first the electronic structure of $TiCp_2Cl_2$ from a qualitative point of view before assigning the Ti 1s excitation spectrum. In this regard, it could seem convenient to consider the effect of substituting a chloride ion with a cyclopentadienyl anion in $TiCpCl_3$. Nevertheless, we believe that a more fruitful strategy is that of starting from the quasi-octahedral $[TiCp_2]^{2+}$fragment,[39] and to look at the perturbations induced by (i) the lowering of θ (the angle between the normals to the Cp rings) and (ii) the addition of two σ donor groups (the chloride ligands).

The quasi-octahedral environment of the Ti atom in the "unbent" $[TiCp_2]^{2+}$ fragment ($\theta = 180°$) splits the empty Ti 3d AOs in t_{2g}-like (d_{xz}, $d_{x^2-y^2}$, and d_{z^2} in our framework—see Figure 1) and e_g-like (d_{xy} and d_{yz}) MOs,[40] with the former set nonbonding and the latter antibonding with respect to the Ti-Cp interaction. A decrease of θ has the primary effect of completely lifting the degeneracy of both sets; in particular, the e_g-like one generates the stabilized $a_2 + b_2$ levels, while the t_{2g}-like set gives rise to the destabilized $1a_1 + b_1 + 2a_1$ orbitals.[39]

When the bent $[TiCp_2]^{2+}$ fragment is allowed to interact with two σ donor ligands in the xz plane, it will use its b_1 orbital and some combination of the $1a_1$ and $2a_1$ ones. Bonding (mainly Cl based) and antibonding (mainly Ti based) combinations will be then originated. On a qualitative basis, one can expect that the Ti 3d-based orbitals of $TiCp_2Cl_2$ will be partitioned in two sets. The former consists of a single a_1 level, while the latter includes four orbitals, two of them (b_2 and a_2) mainly Ti−Cp antibonding in character, the remaining two (b_1 and a_1) antibonding in nature with respect to the Ti−Cl interaction. NR DFT results match quite well such a qualitative picture, even though it is worth noting that the imposition of the C_{2v} symmetry allows an extensive mixing between the $3d_{x^2-y^2}$ and $3d_{z^2}$ AOs which, at variance to results reported by Solomon et al.,[18] equivalently participate (∼30%) to the $24a_1$ and $25a_1$ MOs of Figure 4.

The qualitative description of the $TiCp_2Cl_2$ bonding scheme coupled to results displayed in Figure 2 and 3 allows us to assign the corresponding Ti 1s excitation spectrum. As far as the lowest lying **X′** pre-edge feature is concerned, our results agree with those of Solomon et al.[18] who ascribed it to a transition from the Ti 1s AO to the lowest unoccupied MO (LUMO) constituted, in the C_{2v} symmetry, by a combination of Ti $3d_{x^2-y^2}$ and $3d_{z^2}$ AOs ($1e_{1/2} \rightarrow 64e_{1/2}$ in the C_{2v}* double group, see Table 3). The same agreement does not hold for **X″**: in fact, our results indicate that also **x″** is generated by a single transition, the $1e_{1/2} \rightarrow 67e_{1/2}$ (Ti 1s → Ti $3d_{xz}$), whose *f* value is ∼ twice the one generating **x′**.[41] As far as the onset of the rising edge is concerned, theoretical data suggest to assign it (**y**) to Rydberg transitions mainly involving Ti based AOs ($79e_{1/2} + 81e_{1/2} + 82e_{1/2}$, see Table 3).

TABLE 2: Excitation Energies (eV) and Oscillator Strengths *f* for the Ti 1s Excitation Spectrum of $TiCpCl_3$ from Two Components ZORA TD-DFT[a]

initial state	edge	E (eV)	ΔE (eV)	sym	$f \times 10^4$	TCRFS[(%)b]	SRFS[(%)b,c]
$1s_{1/2}$ ($1\varphi_{1/2}$)	K	4950.3	0.0	a′	0.42422	$55\varphi_{1/2}^{(7)} + 56\varphi_{1/2}^{(93)}$	[21a″(71) + 35a′(29)] + [21a″(26) + 35a′(67) + 36a′(7)]
		4950.3	0.0	a″	0.14224	$55\varphi_{1/2}^{(81)} + 56\varphi_{1/2}^{(19)}$	[21a″(71) + 35a′(29)] + [21a″(26) + 35a′(67) + 36a′(7)]
		4950.3	0.0	a″	0.31378	$55\varphi_{1/2}^{(19)} + 56\varphi_{1/2}^{(81)}$	[21a″(71) + 35a′(29)]+[21a″(26) + 35a′(67) + 36a′(7)]
		4950.4	0.1	a′	0.42049	$57\varphi_{1/2}^{(100)}$	[21″a(3) + 35a′(4) + 36 a′(93)]
		4951.7	1.7	a′	0.39686	$59\varphi_{1/2}^{(100)}$	[22a″(5) + 37a′(95)]
		4951.7	1.7	a″	0.39145	$58\varphi_{1/2}^{(98)} + 59\varphi_{1/2}^{(2)}$	[22a″(95) + 37a′(5)] + [22a″(5) + 37a′(95)]
		4956.3	6.3	a′	0.76422	$68\varphi_{1/2}^{(100)}$	[43a′(100)]
		4957.1	6.8	a′	0.36639	$70\varphi_{1/2}^{(100)}$	[26a″(4) + 44a′(96)]
		4957.1	6.8	a″	0.38488	$69\varphi_{1/2}^{(99)} + 70\varphi_{1/2}^{(1)}$	[26a″(96) + 44a′(4)] + [26a′(4) + 44a′(96)]
		4957.4	7.1	a′	0.24293	$71\varphi_{1/2}^{(100)}$	
		4957.8	7.5	a′	0.15305	$73\varphi_{1/2}^{(100)}$	
		4957.9	7.6	a″	0.49478	$74\varphi_{1/2}^{(100)}$	
		4957.9	7.6	a′	0.80556	$75\varphi_{1/2}^{(100)}$	
		4958.0	7.7	a″	0.67271	$76\varphi_{1/2}^{(100)}$	
		4958.1	7.8	a′	0.24806	$77\varphi_{1/2}^{(100)}$	
		4958.7	8.4	a′	0.85508	$81\varphi_{1/2}^{(25)} + 82\varphi_{1/2}^{(75)}$	
		4958.7	8.4	a′	0.48268	$81\varphi_{1/2}^{(58)} + 82\varphi_{1/2}^{(21)} + 83\varphi_{1/2}^{(21)}$	
		4958.7	8.4	a′	0.29537	$81\varphi_{1/2}^{(16)} + 82\varphi_{1/2}^{(5)} + 83\varphi_{1/2}^{(79)}$	
		4958.8	8.5	a″	0.45574	$84\varphi_{1/2}^{(100)}$	
		4959.0	8.7	a′	1.3080	$86\varphi_{1/2}^{(100)}$	
		4959.0	8.7	a″	0.14818	$85\varphi_{1/2}^{(10)} + 86\varphi_{1/2}^{(90)}$	
		4959.0	8.7	a″	1.5955	$85\varphi_{1/2}^{(90)} + 86\varphi_{1/2}^{(10)}$	
		4959.2	8.9	a′	1.0275	$88\varphi_{1/2}^{(100)}$	
		4959.2	8.9	a′	0.75886	$89\varphi_{1/2}^{(97)} + 91\varphi_{1/2}^{(2)}$	
		4959.3	9.0	a′	0.21479	$89\varphi_{1/2}^{(2)} + 91\varphi_{1/2}^{(97)}$	
		4959.4	9.1	a″	0.21143	$92\varphi_{1/2}^{(100)}$	
		4959.4	9.1	a′	0.25456	$93\varphi_{1/2}^{(98)} + 94\varphi_{1/2}^{(2)}$	
		4959.6	9.3	a′	0.69987	$95\varphi_{1/2}^{(99)} + 96\varphi_{1/2}^{(1)}$	
		4959.7	9.4	a″	0.50934	$97\varphi_{1/2}^{(87)} + 98\varphi_{1/2}^{(13)}$	
		4959.7	9.4	a′	0.23388	$95\varphi_{1/2}^{(1)} + 96\varphi_{1/2}^{(99)}$	
		4959.7	9.4	a′	0.34762	$98\varphi_{1/2}^{(99)} + 99\varphi_{1/2}^{(1)}$	
		4959.7	9.4	a″	0.11390	$97\varphi_{1/2}^{(13)} + 98\varphi_{1/2}^{(87)}$	
		4959.8	9.5	a′	0.16070	$99\varphi_{1/2}^{(2)} + 111\varphi_{1/2}^{(98)}$	

[a] Only the a′ and a″ excitations lying at energies lower than the edge are reported. The DFT−KS 1s ionization energy is 4959.8 eV. TCRFS and SRFS stand for two-component relativistic final state and scalar relativistic final state, respectively. [b] Only transitions having $f \times 10^4 \geq 0.1$ and contributions to the TCRFS/SRFS ≥ 1% are reported. [c] SRFS are reported only for the assigned excitations.

Before addressing the Cl 1s XAS features, it is worth to stress that theoretical distributions of *f* satisfactorily reproduce not only intensities and splittings of Ti 1s structures but also their variations along the series.

Cl K-edges. Normalized Cl K-pre-edge spectra show an evident decrease in the relative intensity along the series,[18] thus indicating a reduction of the Ti−Cl covalency upon substitution of Cl with Cp ligands.[36] Starting with $TiCl_4$, the **X′** and **X″** components of the Cl pre-edge XAS fit[42] are estimated at 2821.58 and 2822.32 eV, respectively, and have their origin in the participation of Cl 3p AOs to the $TiCl_4$ 3e and $10t_2$ MOs. Moreover, the onset of the rising edge is found at ∼5 eV from **X′**. Incidentally, the obtainment of accurate values for $\Delta E_{\mathbf{X''X'}}$ (∼0.7 eV) and $\rho_{\mathbf{X'/X''}}$ (∼0.8) is hampered by the extensive overlap between the two XAS fit components.

SO coupling has no effect on the 1s Cl AOs whose linear combinations transform as a_1 ($e_{1/2}$) + t_2 ($e_{5/2}$ + $u_{3/2}$) in the T_d group (T_d* double group). Calculations have been then carried out by assuming a single IS corresponding to spinors ($2e_{1/2}$ + $1e_{5/2}$ + $1u_{3/2}$). The simulated Cl 1s excitation spectrum of $TiCl_4$ is displayed in Figures 5 and 6, while calculated excitation energies, corresponding intensities and TC-RFS compositions are provided in the Supporting Information (Table S4). Inspection of Figure 5 indicates that the excitation energy region at ∼2800 eV (again the slight underestimation of excitation energies has to be ascribed to deficiencies of the XC potential)[21−22] is characterized by the presence of the peaks **x′** and **x″** at 2799.8 and 2800.7 eV, respectively, whose ΔE (0.87 eV) and $f_{\mathbf{x'}}/f_{\mathbf{x''}}$ (0.57) are in agreement with Solomon results.[18]

Theoretical data allow us to ascribe **x′** to a transition whose TC-RFS is completely localized on the $14u_{3/2}$ (the SR 3e LUMO), while IS contributions from $1e_{5/2}$ and $1u_{3/2}$ spinors amount to 66 and 34%, respectively. At variance to that, two excitations contribute to **x″**, both of them deriving from a strong mixing of configurations involving the second ($10e_{5/2}$) and the third ($15u_{3/2}$) excited states, and both of them related to the SR $10t_2$ MO. Moreover, all Cl 1s based spinors ($2e_{1/2}$ + $1e_{5/2}$ + $1u_{3/2}$) extensively participate to the corresponding ISs. As a whole, these results confirm the already stressed failure of the single particle approach in reproducing XA spectra.

It has been mentioned already that the onset of the rising edge is experimentally found at ∼5 eV from **X′**. Data displayed in Figure 6 prompt us to assign it to the weak feature **y** (the associate excitation energy and the *f* value are 2805.1 eV and 0.93631×10^{-4}, respectively) generated by the ($1e_{5/2}$ + $1u_{3/2}$) → $11e_{1/2}$ Rydberg transition.

Moving from $TiCl_4$ to $TiCpCl_3$, the decrease in relative intensity of the normalized Cl K-edge spectrum (by a factor of 1.17) is accompanied by the splitting of the pre-edge feature in two evident peaks lying at 2821.77 (**X′**) and 2823.13 eV (**X″**), with $\rho_{\mathbf{X'/X''}} = 1.82$ (see Figure 5).[18] Furthermore, the onset of the rising edge is red-shifted by ∼ 0.4 eV.

The analysis of Figure 5 and 6 testifies the agreement between theory and experiment, in fact: i) the simulated Cl K-pre-edge spectrum is characterized by the presence of two peaks (**x′** and **x″**) with a $\Delta E_{\mathbf{x''x'}} = 1.4$ eV, ii) $(f_{\mathbf{x'}} + f_{\mathbf{x''}})^{TiCl_4}/(f_{\mathbf{x'}} + f_{\mathbf{x''}})^{TiCpCl_3} = 1.17$; iii) $(f_{\mathbf{x'}}/f_{\mathbf{x''}})^{TiCpCl_3} = 1.78$; iv) the Cl 1s ionization limit is red-shifted by 0.9 eV.

TABLE 3: Excitation Energies (eV) and Oscillator Strengths *f* for the Ti 1s Excitation Spectrum of $TiCp_2Cl_2$ from Two Components ZORA TD-DFT[a]

initial state	edge	*E* (eV)	Δ*E* (eV)	sym	$f \times 10^4$	TCRFS[(%)b]	SRFS[(%)b,c]
$1s_{1/2}$ ($1e_{1/2}$)	K	4950.0	0.0	a_1	0.20797	$64e_{1/2}^{(100)}$	$[24a_1^{(100)}]$
		4951.2	1.2	b_1	0.36466	$67e_{1/2}^{(100)}$	$[17b_1^{(98)} + 10a_2^{(2)}]$
		4955.8	5.8	a_1	0.27997	$78e_{1/2}$ (1) + $79e_{1/2}$ (99)	$[29a_1^{(99)} + 20b_1^{(1)}] + [30a_1^{(100)}]$
		4955.9	5.9	b_2	0.36094	$81e_{1/2}^{(100)}$	$[19b_2^{(100)}]$
		4956.2	6.2	b_2	0.46644	$82e_{1/2}^{(100)}$	$[20b_2^{(100)}]$
		4956.7	6.7	b_2	0.12702	$85e_{1/2}^{(100)}$	
		4957.0	7.0	a_1	0.14521	$87e_{1/2}^{(100)}$	
		4957.2	7.2	b_1	0.11414	$88e_{1/2}^{(100)}$	
		4957.5	7.5	b_1	0.37133	$90e_{1/2}^{(100)}$	
		4957.7	7.7	a_1	0.13565	$91e_{1/2}^{(100)}$	
		4957.9	7.9	a_1	0.22036	$93e_{1/2}^{(100)}$	
		4958.0	8.0	b_1	0.82804	$94e_{1/2}^{(100)}$	
		4958.2	8.2	b_2	0.20736	$97e_{1/2}^{(100)}$	
		4958.4	8.4	b_1	0.70670	$99e_{1/2}^{(100)}$	
		4958.5	8.5	b_1	0.84678	$104e_{1/2}^{(100)}$	
		4958.5	8.5	a_1	0.31154	$100e_{1/2}^{(12)} + 101e_{1/2}^{(88)}$	
		4958.7	8.7	b_2	0.42777	$105e_{1/2}^{(100)}$	
		4958.8	8.8	b_2	0.11862	$107e_{1/2}^{(100)}$	
		4958.9	8.9	a_1	1.1881	$109e_{1/2}^{(100)}$	
		4959.0	9.0	a_1	0.27588	$111e_{1/2}^{(99)}$	
		4959.1	9.1	b_1	0.29234	$112e_{1/2}^{(100)}$	
		4959.2	9.2	b_1	0.56131	$132e_{1/2}^{(100)}$	
		4959.4	9.4	a_1	0.64302	$133e_{1/2}^{(1)} + 136e_{1/2}^{(98)}$	
		4959.5	9.5	b_1	0.44808	$137e_{1/2}^{(100)}$	
		4959.7	9.7	b_2	1.1217	$139e_{1/2}^{(100)}$	
		4959.8	9.8	a_1	0.46159	$140e_{1/2}^{(99)}$	
		4959.8	9.8	b_1	1.0698	$141e_{1/2}^{(100)}$	

[a] Only the a_1, b_1, and b_2 excitations lying at energies lower than the edge are reported. The DFT−KS 1s ionization energy is 4959.8 eV. TCRFS and SRFS stand for two-component relativistic final state and scalar relativistic final state, respectively. [b] Only transitions having $f \times 10^4 \geq 0.1$ and contributions to the TCRFS/SRFS ≥ 1% are reported. [c] SRFS are reported only for the assigned excitations.

Before going on, it is useful to remind that $\Delta E_{\mathbf{x}''\mathbf{x}'}$ may be associated to the energy difference between e_g- and t_{2g}-like components of Ti 3d AOs in the quasi-octahedral crystal field generated by the Cp ligand and the three chloride anions,[37] and that the corresponding value (1.4 eV) mirrors the one derived from the $TiCpCl_3$ Ti 1s excitation spectrum.

Further details can be obtained by referring to theoretical outcomes ($TiCpCl_3$ excitation energies, corresponding intensities, IS and TC-RFS compositions for a′ and a″ symmetries are provided in the Supporting Information, Tables S5−S6).[43] In particular, they state the following: (i) despite all Cl 1s based spinors ($2\varphi_{1/2} + 3\varphi_{1/2} + 4\varphi_{1/2}$) extensively participate to different ISs, the $2\varphi_{1/2}$ one, associated to the $1s_{1/2}$ spinor of the single chlorine atom (see Figure 1), never mixes with the $3\varphi_{1/2} + 4\varphi_{1/2}$, reminiscent of the in-phase and out-of-phase liner combinations of the symmetry related Cl 1s AOs; (ii) excitations toward lowest lying virtual valence states, spinors $\{55\varphi_{1/2} + 56\varphi_{1/2} + 57\varphi_{1/2}\}$ altogether related to the Ti t_{2g}-like orbitals, imply a strong mixing of configurations in the first ten excited states. Akin considerations hold for excitations toward spinors $\{58\varphi_{1/2} + 59\varphi_{1/2}\}$, on the whole reminiscent of the Ti e_g-like levels, further confirming the inadequacy of a single particle approach in reproducing spectral features. Finally, as far as the onset of the rising edge is concerned, no significant difference is present in the Cl 1s simulated spectrum on passing from $TiCl_4$ to $TiCpCl_3$ (see Figure 6).

The substitution of a chloride ion with a cyclopentadienyl anion in $TiCpCl_3$ further decreases the relative intensity of the $TiCp_2Cl_2$ Cl K-pre-edge spectrum (by a factor of 1.49 with respect to $TiCl_4$) which consists, as in $TiCpCl_3$, of two components (**X′** and **X″**) centered at 2821.27 and 2822.29 eV, but with a reversed peak intensity ratio ($\rho_{\mathbf{X}'/\mathbf{X}''} = 0.40$) (see Figure 5).[18] Moreover, taking $TiCl_4$ as a reference and according to the electron donor properties of Cp ligands, **X′**, **X″**, and the onset of the rising edge are red-shifted.

Again, data reported in Figure 5 and 6 agree quite well with experimental findings.[18] In particular, (i) the simulated Cl K-pre-edge spectrum is characterized by the presence of the peaks **x′** and **x″** with $\Delta E_{\mathbf{x}''\mathbf{x}'} = 1.24$ eV, (ii) $(f_{\mathbf{x}'} + f_{\mathbf{x}''})^{TiCl_4}/(f_{\mathbf{x}'} + f_{\mathbf{x}''})^{TiCp_2Cl_2} = 1.45$, (iii) $(f_{\mathbf{x}'}/f_{\mathbf{x}''})^{TiCp_2Cl_2} = 0.67$, (iv) peaks **x′** and **x″** lye at lower excitation energy (0.92 and 0.58 eV, respectively) than **x′** and **x″** components in $TiCl_4$, and v) the Cl 1s ionization limit is further red-shifted by 1.1 eV on passing from $TiCpCl_3$ to $TiCp_2Cl_2$.

Theoretical data ($TiCp_2Cl_2$ excitation energies, corresponding intensities, IS and TC-RFS compositions for a_1, b_1 and b_2 symmetries are provided in the Supporting Information, Tables S7−S9) encourage us to associate the K-pre-edge feature **x′** to the $2e_{1/2} \rightarrow 64e_{1/2}$ ($f = 1.497 \times 10^{-3}$) and $3e_{1/2} \rightarrow 64e_{1/2}$ ($f = 2.778 \times 10^{-4}$) excitations corresponding, in a SR treatment, to transitions from the in-phase (a_1, the former) and out-of-phase (b_1, the latter) linear combinations of Cl 1s AOs to the $24a_1$ LUMO localized on the Ti $3d_{x^2-y^2}$ (34%) and $3d_{z^2}$ (40%) AOs.[44] As far as the more intense **x″** peak is concerned, (i) at least six excitations, two for each symmetry species a_1, b_1, and b_2 contribute to it, (ii) both the $2e_{1/2}$ and $3e_{1/2}$ spinors participate to the corresponding ISs, and (iii) TC-RFSs stress a significant mixing of configurations. As a final consideration, the presence of several weak excitations beyond those responsible of **x′** and **x″** and having as TC-RFS the high lying $77e_{1/2}$, $78e_{1/2}$, $79e_{1/2}$, and $80e_{1/2}$ virtual valence states are consistent with the shift toward lower excitation energies of the rising edge onset.[45]

Ti L-edges. As already pointed out, the Ti 2p pre-edge excitation spectra are dominated by 2p → 3d transitions. At variance to K-edge spectra, the SO coupling splits the Ti 2p initial levels into $2u_{3/2} + 2e_{5/2}$ in $TiCl_4$, $6\varphi_{1/2} + 7\varphi_{1/2} + 8\varphi_{1/2}$ in $TiCpCl_3$, and $5e_{1/2} + 6e_{1/2} + 7e_{1/2}$ in $TiCp_2Cl_2$. According to that, the most relevant feature of Ti 2p excitation spectra is the presence of two main components (L_3 and L_2) associated to the $2p_{3/2}$ and $2p_{1/2}$ spinors, respectively, with additional

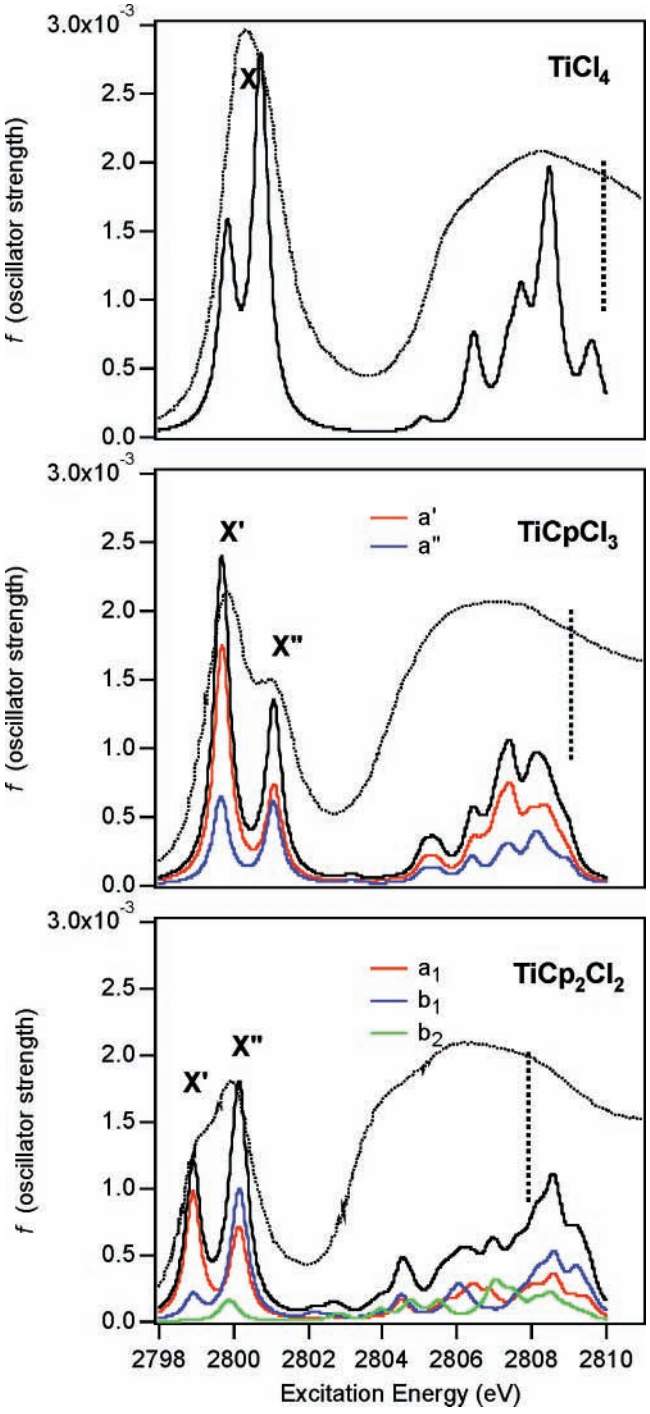

Figure 5. SO-RTDDFT LB94-GS Cl 1s excitation spectra of $TiCl_4$, $TiCpCl_3$, and $TiCp_2Cl_2$. Corresponding electric dipole allowed components are also displayed. Experimental curves (dashed lines) are taken from ref 18, and they are all red-shifted by ~21 eV to allow the matching between the lowest lying theoretical and experimental features. Vertical dotted lines indicate the calculated ionization limits (2810.0, 2809.1, and 2808.0 eV in $TiCl_4$, $TiCpCl_3$, and $TiCp_2Cl_2$, respectively).

weaker structures (see Figure 7). In this regard, it is worthwhile to mention that the energy splitting between $2p_{3/2}$ and $2p_{1/2}$ states is ~6 eV[17] and transitions out from them can be coupled with each other. For this reason, and analogously to the calculations carried out by Fronzoni et al.[21] to simulate the $TiCl_4$ $L_{2,3}$ edges, the whole Ti $2p_{3/2}/2p_{1/2}$ set was considered as initial state.[46]

The **X′** and **Y′** main lines of the $TiCpCl_3$ Ti 2p spectrum lie at 458.6 and 464.0 eV, respectively; moreover, both features consist of two components and additional weaker structures (see Figure 7).[17] In more detail, a well resolved peak is present on

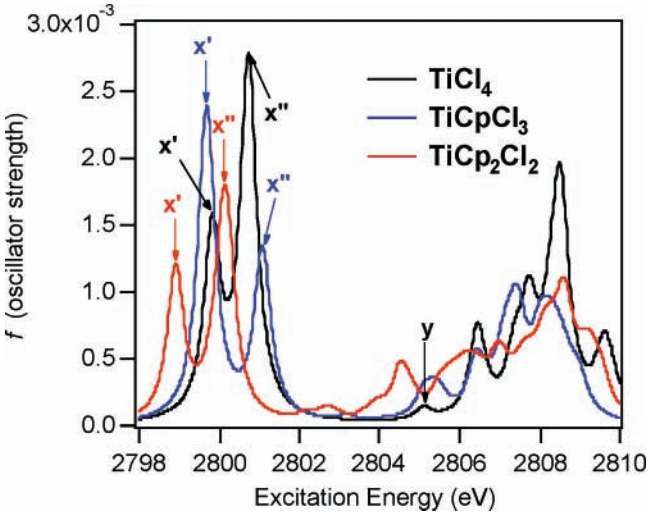

Figure 6. Superposition of the SO-RTDDFT LB94-GS Cl 1s excitation spectra of $TiCl_4$, $TiCpCl_3$, and $TiCp_2Cl_2$.

the lower excitation energy side of **X′** at 457.0 eV (X, in Figure 7), while the L_2 feature, besides the shoulder **S** at 462.7 eV, is characterized by two weak and broad bands at ~467 and ~472 eV, and ascribed by Wen and Hitchcock[17] to L_3 (the former) and L_2 (the latter) double excitations. Furthermore, even though they did not report any quantitative estimate of peak relative intensities, Figure 5 of their contribution clearly shows that $\rho_{X/X'}$ significantly increases on passing from $TiCl_4$ to $TiCpCl_3$. Finally, it has to be remarked that Wen and Hitchcock[17] claimed the presence of a further L_3-based feature at 460.8 eV which is actually not very clear in their $TiCpCl_3$ 2p *f* spectrum.

Calculations on $TiCpCl_3$ fit very well experimental evidence.[17] In particular, the L_3 excitation energy region of the simulated spectrum is characterized by the presence of three peaks (**x**, **x′**, and **x″** at 453.5, 455.0, and 456.6 eV, respectively; see Figure 8) whose relative energy positions nicely match experimental data. Moreover, in agreement with experimental evidence, $f_x/f_{x'}$ passes from 0.13 in $TiCl_4$ to 0.46 in $TiCpCl_3$. As far as the L_2 excitation energy region of the simulated spectrum is concerned, it consists of peaks **y**, **y′** (at 459.2 and 460.6 eV, respectively) and of the broad structure **y″** centered at ~ 461.5 eV. Both $\Delta E_{y'x'} = 5.54$ eV and $\Delta E_{y'y} = 1.38$ eV, corresponding to ΔEs between L_2 and L_3 main components, and between L_2 and the shoulder on its lower excitation energy, respectively, reproduce almost quantitatively the experimental values of 5.40 and 1.3 eV. Interestingly, the $2p_{3/2}$-based spinors ($7\varphi_{1/2} + 8\varphi_{1/2}$) contribute not only to the L_3 region, but extend their participation to the L_2 one. Such a result is in tune with data reported by the Sawatzky group[47] and it provides a first principle rationale for deviations from the expected $\rho(L_3/L_2)$ (2:1).[48]

Moving to the assignment of the $TiCpCl_3$ Ti-2p *f* spectrum, our results indicate that both **x** and **x′** originate from three excitations whose corresponding transitions have as IS almost pure $2p_{3/2}$-based spinors. As far as the corresponding TC-RFS are concerned, it deserves to be emphasized that even though they are characterized by a strong mixing of configurations implying all the excited states ($55\varphi_{1/2}-59\varphi_{1/2}$) related to the Ti 3d-based virtual levels (35a′−37a′ + 21a″−22a″), contributions to **x** (**x′**) from excitations involving Ti t_{2g}-based (Ti e_g-based) 35a′−36a′ + 21a″ (37a′ + 22a″) MOs exceed the 70% (80%). Finally, the $\rho_{X/X'}$ low value has to be ultimately traced back to the oscillator strengths of excitations contributing to **x** (1.6966×10^{-2}; 2.3459×10^{-2}; 2.3465×10^{-2}) and **x′** (5.3348×10^{-2}; 5.2850×10^{-2}; 6.7875×10^{-2}).

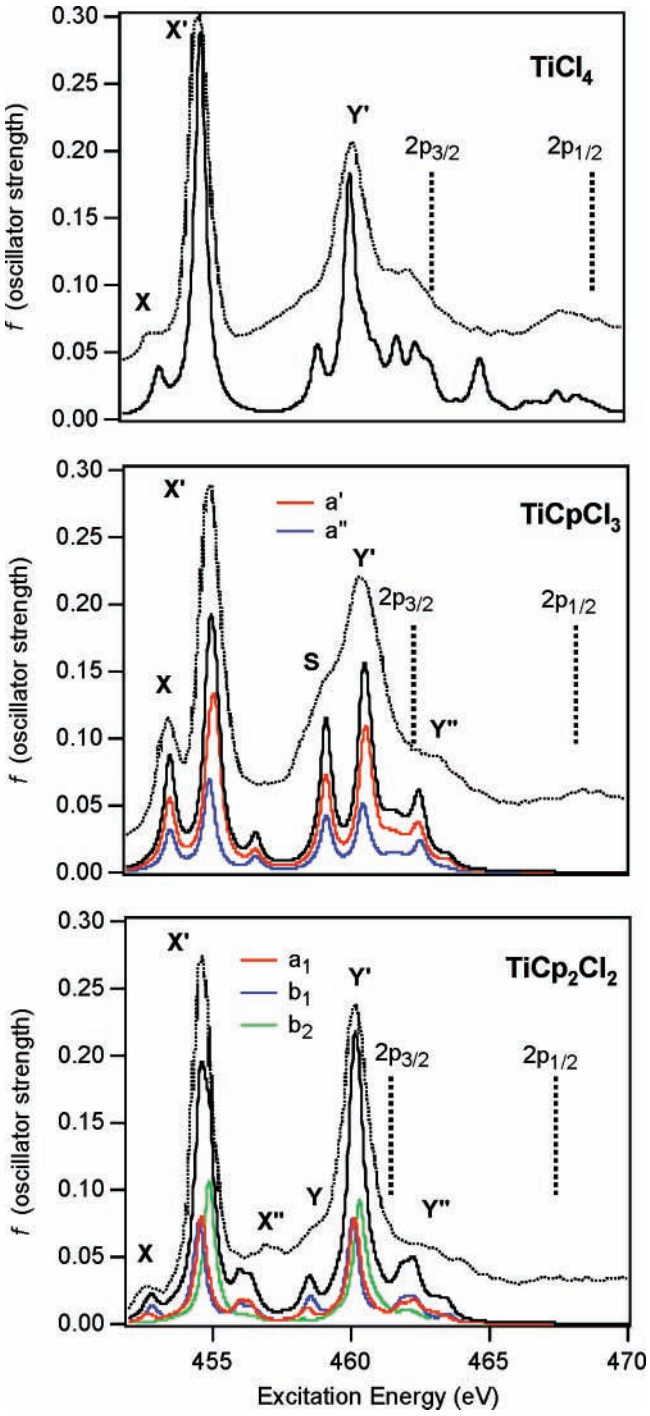

Figure 7. SO-RTDDFT LB94-GS Ti 2p excitation spectra of $TiCl_4$, $TiCpCl_3$, and $TiCp_2Cl_2$. Corresponding electric dipole allowed components are also displayed. Experimental curves (dashed lines) are taken from ref 17, and they are all red-shifted by ~4 eV to allow the matching between the lowest lying theoretical and experimental features. Vertical dotted lines indicate the calculated $2p_{3/2}$ (463.2, 462.4, 461.5 eV) and $2p_{1/2}$ (469.0, 468.3, 467.5 eV) ionization limits in $TiCl_4$, $TiCpCl_3$, and $TiCp_2Cl_2$.

On passing from $TiCl_4$ to $TiCpCl_3$, a new **x″** peak (at 3.1 eV from **x**) appears in the L_3 region of the simulated excitation spectrum. We tentatively assign it to the feature found by Wen and Hitchcock[17] at 460.8 eV in the $TiCpCl_3$ Ti 2p *f* spectrum. In this regard, it is worth noting that **x″** is due to two excitations having (i) almost pure $2p_{3/2}$-based spinors as ISs, (ii) *f* values equal to 0.87476×10^{-2} and 0.79102×10^{-2}, and (iii) TC-RFS constituted by two combinations of the $60\varphi_{1/2}$ and $61\varphi_{1/2}$

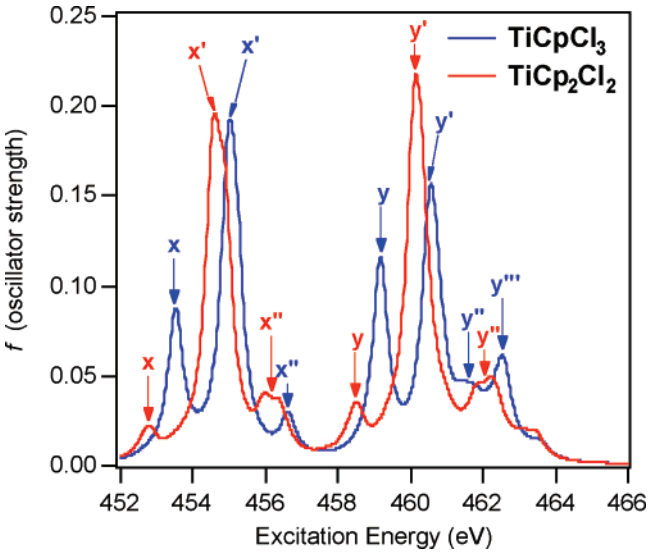

Figure 8. Superimposition of the SO-RTDDFT LB94-GS Ti 2p excitation spectra of $TiCpCl_3$ and $TiCp_2Cl_2$.

spinors corresponding to S-RFS 38a′ + 23a″ virtual levels which, among Cp based π^* MOs, are those with largest, even though amounting to a few percents, contributions from Ti 3d AOs. Interestingly, the $\Delta E_{x''x}$ value agrees semiquantitatively[49] with the ΔE (2.5 eV) between those peaks of the C 1s *f* spectrum assigned by Wen and Hitchcock to C 1s → Cp π^* MOs and C 1s → Ti t_{2g}-like transitions.[17]

Among the excitations generating **y**, **y′**, and the broad structures **y″** and **y‴** (see Figure 8), only those giving rise to **y** (three) correspond to transitions having the $2p_{1/2}$ spinor as IS. Moreover, as already found for **x**, the TC-RFS of these transitions implies a strong mixing of Ti 3d-based spinors ($55\varphi_{1/2}$–$57\varphi_{1/2}$) reminiscent of the S-RFS t_{2g}-based MOs (35a′-36a′ + 21a″ levels). At variance to that, **y′**, **y″**, and **y‴** structures include L_3 Rydberg transitions which overlap with valence excitations of the L_2 edge. More specifically, among the eight excitations contributing to **y′** only one can be associated to a transition from the $6\varphi_{1/2}$ spinor to strongly mixed Ti e_g-based spinors (the $58\varphi_{1/2}$–$59\varphi_{1/2}$ ones), while the remaining seven have large Ti Rydberg contributions (essentially Ti 4p).

Three excitations characterized by low oscillator strengths ($f < 10^{-1}$) fall in the energy region covered by the broad structure **y″** and all of them correspond to L_3 Rydberg transitions converging to the L_3 threshold. Finally, two excitations from the Ti 2p-based $6\varphi_{1/2}$ spinor to excited states represented by combinations of the above-described $60\varphi_{1/2}$ and $61\varphi_{1/2}$ belongs to **y‴**.

The Ti 2p *f* spectra of $TiCpCl_3$ and $TiCp_2Cl_2$ are quite similar, even though an overall red shift, ranging from 0.5 to 1.2 eV, is imposed on the spectral features upon substitution of a chloride ion with the cyclopentienyl anion (see Figure 7 and 8). According to that, the Ti 2p *f* spectrum of $TiCp_2Cl_2$ consists of two main components (**X′** and **Y′** at 457.9 and 463.5 eV, respectively). Additional weaker and ill resolved structures are also present on both sides of **X′** (**X** and **X″** at 455.8 and 460.3 eV, respectively) and **Y′** (**Y**, **Y″**, and **Y‴** at 462.0, 466, and 471.5 eV, respectively).[17] Moreover, a significant decrease of $\rho_{X/X'}$ and $\rho_{Y/Y'}$ ratios is well evident on passing from $TiCpCl_3$ to $TiCp_2Cl_2$.

Theoretical calculations on the $TiCp_2Cl_2$ molecule reveal a good agreement between theory and experiment. Actually, both the L_3 and L_2 energy regions are characterized by the presence of three structures (**x**, **x′**, **x″** and **y**, **y′**, **y″** in Figure 8) lying at

452.8, 454.6, 456.1 and 458.5, 460.2, 462.1 eV, respectively. In this regard, it has to be stressed that (i) $\Delta E_{\mathbf{y'x'}}$ (5.54 eV), $\Delta E_{\mathbf{x'x}}$ (1.8 eV), $\Delta E_{\mathbf{y'y}}$ (1.7 eV) reproduce almost quantitatively experimental evidence and (ii) $f_{\mathbf{x}}/f_{\mathbf{x'}}$ (0.12) and $f_{\mathbf{y}}/f_{\mathbf{y'}}$ (0.16) are compatible with the $TiCp_2Cl_2$ 2p *f* spectrum.[17] The agreement between experiment and theory is less satisfactory when **x″** and **y″** features are considered (see Figure 7).[49]

We are now ready to tackle the assignment of the $TiCp_2Cl_2$ Ti 2p spectral features. The theoretical calculations indicate that both **x** and **x′** arise from the following transitions: two for **x** (of symmetry a_1 and b_1) and four for **x′** ($2a_1$, b_1, and b_2),[50] from $2p_{3/2}$-based spinors to Ti 3d-based MOs. Interestingly, excitations generating **x** have the same TC-RFS (the already described $64e_{1/2}$ spinor, see Table 3),[51] while they differ for the $6e_{1/2}$ and $7e_{1/2}$ contributions to ISs. At variance to that, TC-RFS of excitations associated to **x′** are all characterized by a strong mixing of configurations involving the 65-$68e_{1/2}$ spinors tightly related to the four Ti 3d based.[43] In this regard, we point out that (i) both the higher number of excitations contributing to **x′** and the corresponding *f* values concur to determine the low $f_{\mathbf{x}}/f_{\mathbf{x'}}$ and (ii) the qualitative bonding scheme proposed for $TiCp_2Cl_2$ just on the basis of symmetry arguments and overlap considerations nicely matches the experimental evidence so far considered.

As far as the assignment of **x″** is concerned, the first thing to be remarked is that its origin is closely related to the **x″** structure of the $TiCpCl_3$ Ti 2p *f* simulated spectrum. In the present case, four transitions from pure $2p_{3/2}$-based spinors to combinations of the $69e_{1/2}-71e_{1/2}$ spinors are involved, even if the excitations with the highest *f* involve the $69e_{1/2}$ and $71e_{1/2}$ spinors (SR $18b_1$ and $26a_1$ MOs, respectively) which have the largest, even if skinny, contribution from Ti 3d AOs.

Despite the above-mentioned similarity between $TiCpCl_3$ and $TiCp_2Cl_2$ Ti 2p excitation spectra, the assignment of the $TiCp_2Cl_2$ y feature is quite different from that proposed for the three-chloride derivative. Actually, two excitations, of symmetry b_1 and a_1, and both associated to the $5e_{1/2} \rightarrow 64e_{1/2}$ transition contribute to it.

According to its higher intensity, several excitations concur to **y′**, even though only those ($a_1 + 2b_1 + b_2$) deriving from transitions having the Ti $2p_{1/2}$ spinor as initial state and TC-RFS made of strongly mixed configurations of the $65e_{1/2}-68e_{1/2}$ spinors have a *f* value higher than 0.1×10^{-1}. A large number of excitations with *f* values lower than 10^{-1} contribute to **y″**. Many of them correspond to transitions from Ti $2p_{3/2}$ spinors to high lying excited states, even though it worth noting that the $5e_{1/2}$ participation to ISs always implies contributions from the $5e_{1/2} \rightarrow 69e_{1/2}$ and $5e_{1/2} \rightarrow 71e_{1/2}$ transitions.

As a whole these results confirm that the $2p_{3/2}$-based spinors contribute not only to the L_3 region, but extend their participation to the L_2 one thus providing, also in this case, a rationale for deviations from the expected $\rho(L_3/L_2)$ (2:1).

4. Concluding Remarks

Ti 1s, Cl 1s and Ti 2p ($L_{2,3}$) core excitation spectra of $TiCl_4$, $TiCpCl_3$, and $TiCp_2Cl_2$ have been assigned by using the state-of-the-art approach to theoretically describe XAS data, i.e., the two-components ZORA SO-RTDDFT method implemented in the ADF package. Simulated *f* distributions along the investigated series were able to satisfactorily reproduce the relative intensities of title molecule spectral features.

Our results for $TiCpCl_3$ and $TiCp_2Cl_2$ substantially confirm previous assignments based either on empirical methods[17] or ground state DFT calculations.[18] Nevertheless, it is shown that the use of SO-RTDDFT brings significant improvement in the assignment of XAS features.

Acknowledgment. The Laboratorio Interdipartimentale di Chimica Computazionale (LICC) dell'Università di Padova is acknowledged for support of the computer facilities. We thank G. Fronzoni and M. Stener for the helpful discussions.

Supporting Information Available: Optimized Cartesian coordinates of $TiCpCl_3$ and $TiCp_2Cl_2$ obtained by assuming C_s and C_{2v} symmetry. Excitation energies, *f* values, and TC-RFS for Cl 1s excitation spectra of $TiCl_4$, $TiCpCl_3$, and $TiCp_2Cl_2$ and Ti 2p excitation spectra of $TiCpCl_3$ and $TiCp_2Cl_2$. This material is available free of charge via the Internet at http://pubs.acs.org.

References and Notes

(1) Dewar, M. J. S. *Bull. Soc. Chim. Fr.* **1951**, *18*, C71.
(2) Chatt, J.; Duncanson, L. A. *J. Chem. Soc.* **1953**, 2939.
(3) Chatt, J.; Dilworth, J. R.; Richards, R. L. *Chem. Rev.* **1978**, *78*, 589. (b) Lukehart, C. M. *Fundamental Transition Metal Organo-metallic Chemistry*; Brooks/Cole: Monterey, CA, 1985. (c) Hartley, F. R. In *Comprehensive Organometallic Chemistry*; Wilkinson, G., Ed.; Pergamon: Oxford, U.K., 1982; Vol. 6. (d) Veillard, A. *Chem. Rev.* **1991**, *91*, 743. (e) Koga, N.; Morokuma, K. *Chem. Rev.* **1991**, *91*, 823. (f) Li, J.; Schreckenbach, G.; Ziegler, T. *J. Chem. Phys.* **1994**, *98*, 4838. (g) Li, J.; Schreckenbach, G.; Ziegler, T. *J. Am. Chem. Soc.* **1995**, *117*, 486. (h) Jacobsen, H.; Schreckenbach, G.; Ziegler, T. *J. Phys. Chem.* **1994**, *98*, 11406. (i) Li, J.; Schreckenbach, G.; Ziegler, T. *Inorg. Chem.* **1995**, *34*, 3245. (j) Niu, S.; Hall, M. B. *Chem. Rev.* **2000**, *100*, 353. (k) Dedieu, A. *Chem. Rev.* **2000**, *100*, 543. (l) Frenking, G.; Fröhlich, N. *Chem. Rev.* **2000**, *100*, 717.
(4) *Chem. Rev.* **2000**, *100* (4).
(5) Mono- and bis-cyclopentadienyltitanium(IV) complexes act as homogeneous polymerization catalysts[6−7] and present several advantages when compared with traditional Ziegler−Natta catalysts.[8] In particular, they are homogeneous single active sites of very high activity that may be heterogenized to provide further advantages in terms of control of polymer properties, activity, and microstructure.
(6) Qian, Y.; Huang, J.; Bala, M. D.; Lian, B.; Zhang, H.; Zhang, H. *Chem. Rev.* **2003**, *103*, 2633, and references therein.
(7) (a) Longo, P.; Grassi, A.; Oliva, L. *Makromol. Chem.* **1990**, *191*, 2387. (b) Pellecchia, C.; Oliva, L. *Rubber Chem. Technol.* **1999**, *72*, 553.
(8) Natta, G. *Angew. Chem.* **1956**, *68*, 393.
(9) Guo, M.; Sun, H.; McArdle, H. J.; Gambling, L.; Sadler, P. J. *Biochemistry* **2000**, *39*, 10023.
(10) Boyles, J. R.; Baird, M. C.; Campling, B. G.; Jain, N. J. *Inorg. Biochem.* **2001**, *84*, 159.
(11) The absorption edges are labeled in the order of increasing energy, K, L_1, L_2, L_3, M_1, ..., corresponding to the excitation of an electron from the 1s ($S_{1/2}$), 2s ($S_{1/2}$), 2p ($P_{1/2}$), 2p ($P_{3/2}$), 3s ($S_{1/2}$), ... orbitals (states), respectively.
(12) Douglas, B. E.; Hollingsworth, C. A. *Symmetry in Bonding and Spectra, an Introduction*; Academic Press, Inc.: Orlando, 1985; pp 256−257.
(13) Electric quadrupole transitions involve states of the same parity and they are ~2 orders of magnitude weaker than electric dipole transitions.
(14) Hahn, J. E.; Scott, R. A.; Hodgson, K. O.; Doniach, S.; Desjardins, S. R.; Solomon, E. I. *Chem. Phys. Lett.* **1982**, *88*, 595.
(15) (a) Solomon, E. I.; Hedman, B.; Hodgson, K. O.; Dey, A.; Szilagyi, R. K. *Coord. Chem. Rev.* **2005**, *249*, 97, and references therein reported. (b) Glaser, T.; Hedman, B.; Hodgson, K. O.; Solomon, E. I. *Acc. Chem. Res.* **2000**, *33*, 859.
(16) Kuetgens, U.; Hormes, J. *SIF Conf. Proc.* **1990**, *25*, 59.
(17) Wen, A. T.; Hitchcock, A. P. *Can. J. Chem.* **1993**, *71*, 1632.
(18) De Beer George, S.; Brant, P.; Solomon, E. I. *J. Am. Chem. Soc.* **2005**, *127*, 667.
(19) (a) te Velde, G.; Bickelhaupt, F. M.; Baerends, E. J.; Guerra, C. F.; van Ginsberg, S. J. A.; Snijders, J. G.; Ziegler, T. *J. Comput. Chem.* **2001**, *22*, 931. (b) Baerends, E. J.; Ellis, D. E.; Ros, P. *Chem. Phys.* **1973**, *2*, 41.
(20) Stener, M.; Fronzoni, G.; de Simone, M. *Chem. Phys. Lett.* **2003**, *373*, 115.
(21) Fronzoni, G.; Stener, M.; Decleva, P.; Wang, F.; Ziegler, T.; van Lenthe, E.; Baerends, E. J. *Chem. Phys. Lett.* **2005**, *416*, 56.
(22) Wang, F.; Ziegler, T.; van Lenthe, E.; van Gisbergen, S.; Baerends, E. J. *J. Chem. Phys.* **2005**, *122*, 204103, and references therein.

(23) Amsterdam Density Functional (ADF) version 2006.01. http://www.scm.com.

(24) (a) van Lenthe, E.; Baerends, E. J.; Snijders, J. G. *J. Chem. Phys.* **1993**, *99*, 4597. (b) van Lenthe, E.; Baerends, E. J.; Snijders, J. G. *J. Chem. Phys.* **1994**, *101*, 9783. (c) van Lenthe, E.; Ehlers, A. W.; Baerends, E. J.; Snijders, J. G. *J. Chem. Phys.* **1999**, *110*, 8543.

(25) van Lenthe, E.; Baerends, E. J. *J. Comput. Chem.* **2003**, *24*, 1142.

(26) Gross, E. K. U.; Kohn, W. *Adv. Quantum Chem.* **1990**, *21*, 255.

(27) van Leeuwen, R.; Baerends, E. J. *Phys. Rev. A* **1994**, *49*, 2421.

(28) van Lenthe, J. H.; Faas, S.; Snijders, J. G. *Chem. Phys. Lett.* **2000**, *328*, 107.

(29) A further calculation on $TiCp_2Cl_2$ with Cp rings in a staggered configuration and a C_s symmetry has been also carried out. Optimized coordinates for $TiCpCl_3$ (C_s symmetry) and $TiCp_2Cl_2$ (C_s and C_{2v} symmetry) are provided in the Supporting Information.

(30) Vosko, S. H.; Wilk, L.; Nusair, M. *Can. J. Phys.* **1980**, *58*, 1200.

(31) (a) Becke, A. D. *Phys. Rev. A.* **1988**, *38*, 3098. (b) Perdew, J. P. *Phys. Rev. B* **1986**, *33*, 8822.

(32) Ti-based s, p, and d AOs span the a_1 ($e_{1/2}$), t_2 ($u_{3/2} + e_{5/2}$), and $e + t_2$ ($2u_{3/2} + e_{5/2}$) irreducible representations of the T_d group (T_d* double group), respectively; the a_1 ($e_{1/2}$), $a_1 + b_1 + b_2$ ($3e_{1/2}$); $2a_1 + a_2 + b_1 + b_2$ ($4e_{1/2}$) irreducible representations of the C_{2v} group (C_{2v}* double group), respectively; the a′ ($a_{1/2} + a_{1/2}$*), 2a′ + a″ ($3a_{1/2} + 3a_{1/2}$*), 3a′ + 2a″ ($5a_{1/2} + 5a_{1/2}$*) irreducible representations of the C_s group (C_s* double group), respectively. Hereafter, ($a_{1/2} + a_{1/2}$*) will be indicated by $\varphi_{1/2}$. The complete set of multiplication tables of the thirty-two point groups can be found in ref. 33

(33) Koster, G. F.; Dimmock, J. O.; Wheeler, R. G.; Statz, H. *Properties of the Thirty-Two Point Groups*: M.I.T. Press: Cambridge, MA, 1963.

(34) The inclusion of relativistic effects allows a very good agreement between experiment[16,18] and theory for both excitation and ionization energies (the NR DFT Kohn Sham−DFT-KS−ionization limit is 4897.6 eV,[20] while the experimental value is 4977 eV).[16]

(35) Solomon et al.[18] pointed out that, beside the L-assisted Ti 4p−3d mixing, the Ti K-pre-edge feature could gain intensity through a quadrupole mechanism, estimating the corresponding contribution to ∼10%.

(36) The origin of the pre-edge intensity decreasing in the Ti and Cl 1s excitation spectra along the investigated series has been thoroughly discussed in ref. 18.

(37) Elian, M.; Chen, M. M. L.; Mingos, D. M. P.; Hoffmann, R. *Inorg. Chem.* **1976**, *15*, 1148.

(38) The determination of the actual position of the **X′** component in the Ti 1s excitation spectrum of $TiCp_2Cl_2$ is not straightforward since it has been determined by means of a fitting procedure.

(39) Lauher, J. W.; Hoffmann, R. *J. Am. Chem. Soc.* **1976**, *98*, 1729.

(40) In the actual D_{5h} symmetry, t_{2g}- and e_g-like MOs of the unbent $[TiCp_2]^{2+}$ fragment transform as $e_{2g} + a_{1g}$ and e_{1g}, respectively.

(41) The contribution of the Ti $3d_{xy}$ orbital to the $67e_{1/2}$ spinor is negligible. Moreover, the *f* values of the $1e_{1/2} \rightarrow 65e_{1/2}$ transition (4951.0 eV), reminiscent of the Ti $1s \rightarrow 3d_{yz}$ one, are 1.4700×10^{-8} (a_1), 2.8234×10^{-8} (b_1), and 2.1531×10^{-6} (b_2).

(42) Solomon et al. 18 pointed out that Cl K-pre-edge data always need at least two peaks (**X′** and **X″**) to be fit.

(43) Calculations have been carried out by assuming a single IS corresponding to Cl 1s based spinors ($2\varphi_{1/2} + 3\varphi_{1/2} + 4\varphi_{1/2}$).

(44) Spinors $64e_{1/2}$, $65e_{1/2}$, $66e_{1/2}$, $67e_{1/2}$, and $68e_{1/2}$ are related to the SR $24a_1$, $16b_2$, $10a_2$, $17b_1$, and $25a_1$ Ti 3d-based MOs, respectively.

(45) Spinors $77e_{1/2}$, $78e_{1/2}$, $79e_{1/2}$, and $80e_{1/2}$ are related to SR $20b_1$, $29a_1$, $30a_1$, and $12a_2$ MOs. With the exception of the $30a_1$ level, strongly localized on the Ti 4s AO, the remaining ones are mainly Cp-based.

(46) Theoretical results pertaining to the $TiCl_4$ Ti 2p excitation spectrum substantially match the ones of ref. 21 making needless their detailed description.

(47) (a) Fink, J.; Müller-Heinzerling, Th.; Sheerer, B.; Speier, W.; Hillebrecht, F. U.; Fuggle, J. C.; Zaanen, J.; Sawatzky, G. A. *Phys. Rev. B* **1985**, *32*, 4899. (b) Zaanen, J.; Sawatzky, G. A.; Fink, J.; Speier, W.; Fuggle, J. C. *Phys. Rev. B* **1985**, *32*, 4905. (c) de Groot, F. M. F.; Fuggle, J. C.; Thole, B. T.; Sawatzky, G. A. *Phys. Rev. B* **1990**, *41*, 928.

(48) The experimental relative intensity of L_3 ($2p_{3/2}$) and L_2 ($2p_{1/2}$) features in $TiCpCl_3$ and $TiCp_2Cl_2$ is about 1:1, i.e., much smaller than the 2:1 value associated to the degeneracy of the $^2P_{3/2}$ and $^2P_{1/2}$ ion states.

(49) It has to be kept in mind that the C basis set does not include diffuse functions.

(50) One of the a_1 excitations, that lying at 453.68 eV, is characterized by a very small *f* value (0.1168×10^{-2} in Table S12).

(51) The contribution of the $64e_{1/2}$ spinor to the first two excited states is ∼90%.